



# Fabrication and enhanced supercapacitive performance of sulfur and nitrogen co-doped porous graphene

Xuesha Zhang<sup>1</sup> · Ruijun Zhang<sup>1</sup> · Yanyan Liu<sup>1</sup> · Kang Liu<sup>1</sup> · Yu Gu<sup>1,2</sup> · Ting Liu<sup>1</sup> · Mengjie Liu<sup>1</sup> · Wenyu Wu<sup>1</sup>

Received: 6 September 2017 / Accepted: 24 November 2017 / Published online: 2 December 2017  
© Springer Science+Business Media, LLC, part of Springer Nature 2017

## Abstract

In this paper, we present a strategy to prepare the sulfur and nitrogen co-doped porous graphene electrode, in which, three main procedures—the pore-formation in the natural graphite, the preparation of sulfur doped porous graphite intercalation compounds (S-PGIC) and the construction of the sulfur/nitrogen co-doped porous reduced graphite oxide (SN-PRGO) are included. The as-prepared SN-PRGO sample can behave relatively high specific surface area (SSA) and simultaneously provide through-plane and in-plane diffusion paths for electrolyte ions, thus exhibiting an outstanding capacitive performance. Its specific capacitance at the scan rate of  $5 \text{ mV s}^{-1}$  in 6 M KOH aqueous electrolyte can reach up to  $438 \text{ F g}^{-1}$ , which is, to the best of our knowledge, among the highest values so far reported for heteroatoms doped carbon materials. Besides, SN-PRGO also exhibits an excellent cycling stability with almost 94% of its initial capacitance being retained after the long-term consecutive cycling. This work suggests that constructing the doped graphene-based materials by generating the pores in the graphite sheets and using the intercalated substances among the graphite layers as the dopant sources can be considered as a promising strategy for the development of high performance electrodes in supercapacitors.

## 1 Introduction

Graphene has been considered as a promising candidate electrode material for supercapacitors due to its high theory surface area, excellent electrical conductivity and stable chemical properties [1, 2]. In fact, however, the capacitive performance of graphene is far poorer than the expected. Since the device energy density is generally limited by the capacitance of the graphene electrode [3–5], it will be of great value to develop the strategy that enhances the capacitive performance of the graphene for its practical application in the field.

Recent studies have shown that chemical doping the graphene with heteroatoms could improve the electrochemical

properties effectively, since the incorporation of heteroatoms can contribute both the pseudocapacitance through the redox reaction between the heteroatom-containing functional groups and electrolyte ions as well as the EDLC capacitance by the improvement in the charge mobility and wettability with electrolytes [6–9]. To date, the doping candidates, including S, N, P and so on, have been reported, which are mostly incorporated by post-treating graphene oxide or reduced graphene oxide with dopants [6, 10, 11]. In our previous work [12], we propose a different sulfur and nitrogen co-doping graphene strategy. Significantly different from those conventional routes of doping graphene oxide or reduced graphene oxide, we utilize for the first time the intercalated  $\text{H}_2\text{SO}_4$  among the natural graphite layers as the doped S source, and, the resultant S/N co-doped graphene behaves a great improvement in the capacitive performance.

However, it is noteworthy that, for the graphene—a 2D planar architecture nanomaterial, its through-plane diffusivity is rather low due to the lack of pores in the relative intact structure of graphene sheets [13–15], which will undoubtedly be unfavorable to the fast ion diffusion in the through-plane direction and thus the achievement of high capacitance and excellent rate performance.

To address the problem, herein, we propose a strategy to construct the sulfur and nitrogen co-doped porous graphene

**Electronic supplementary material** The online version of this article (<https://doi.org/10.1007/s10854-017-8323-2>) contains supplementary material, which is available to authorized users.

✉ Ruijun Zhang  
zhangrj@ysu.edu.cn

<sup>1</sup> State Key Laboratory of Metastable Materials Science and Technology, Yanshan University, Qinhuangdao 066004, China

<sup>2</sup> Qian'an College, North China University of Science and Technology, Tangshan 063009, China

(Scheme 1). Firstly, the porous structure in natural graphite is generated by KOH etching. Secondly, the resultant porous graphite is intercalated with sulfuric acid and then thermally treated, achieving a sulfur doped porous graphite intercalation compounds (S-PGIC). Finally, the sulfur and nitrogen co-doped porous reduced graphene oxide (SN-PRGO) is constructed by oxidizing S-PGIC using the modified Hummers' method and then reduction with hydrazine hydrate. This architecture can behave relatively high specific surface area (SSA) and simultaneously provide through-plane and in-plane diffusion path for electrolyte ions. Furthermore, the co-incorporation of sulfur and nitrogen in the porous graphene can be expected to further enhance the supercapacitive performances.

## 2 Experimental

### 2.1 Sample preparation

#### 2.1.1 Preparation of porous nature graphite (PNG)

10 g nature graphite (NG) powder was impregnated in 500 ml KOH aqueous solution with a 14 M concentration for 12 h at room temperature. The extra KOH solution was removed by briefly filtering the mixture through a polycarbonate membrane (Whatman, 0.2  $\mu\text{m}$ ), and then the mixture was dried at 80  $^{\circ}\text{C}$  for 12 h. Thereafter, the dried graphite with attached KOH powder was heated from room temperature to 200  $^{\circ}\text{C}$  at 1  $^{\circ}\text{C min}^{-1}$  and kept at 200  $^{\circ}\text{C}$  for 30 min. Subsequently, the temperature was further increased to a predetermined final temperature of 800  $^{\circ}\text{C}$  at a heating rate of 10  $^{\circ}\text{C min}^{-1}$  and held for 1 h. The whole KOH-etching process was carried out in argon atmosphere. The product after the etching were thoroughly washed with 0.1 M HCl

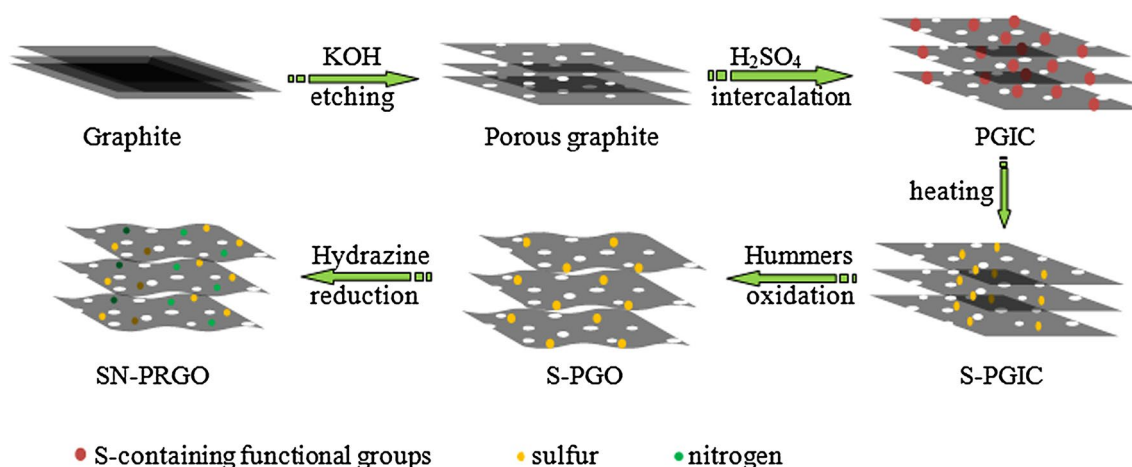
and finally by deionized water to remove the residual K compounds until the pH value of the washed solution was 7. Finally, the product was dried at 80  $^{\circ}\text{C}$  for 12 h, thus obtaining the porous nature graphite (PNG).

#### 2.1.2 Preparation of sulfur doped porous graphite intercalation compound (S-PGIC)

3 g PNG powder and 15 ml  $\text{H}_2\text{SO}_4$  was added to a beaker, followed by a slowly addition of 2.5 ml  $\text{H}_2\text{O}_2$ . Then, the resultant mixture was magnetically stirred at 30  $^{\circ}\text{C}$  for 3 h. Finally, the mixture was placed in a quartz boat and introduced into a horizontal tubular furnace heated to 1000  $^{\circ}\text{C}$  for 2 h under argon atmospheric pressure, thus achieving the sulfur doped porous graphite intercalation compound (S-PGIC).

#### 2.1.3 Preparation of sulfur and nitrogen co-doped porous graphene (SN-PRGO)

The sulfur doped porous graphite oxide (S-PGO) was acquired by the modified Hummers' method [16]. Briefly, 1.5 g S-PGIC powder, 1 g  $\text{NaNO}_3$  and 46 ml  $\text{H}_2\text{SO}_4$  (98%) were stirred in a 250 ml flask in ice bath for 1 h. And then, 6 g  $\text{KMnO}_4$  was slowly added to the solution. After that, the solution was placed in a 35  $^{\circ}\text{C}$  water bath for another 2 h, followed by a slowly addition of 80 ml deionized water. Thereafter, the temperature of the solution was raised to 90  $^{\circ}\text{C}$  and maintained for 0.5 h. Next 60 ml deionized water and 30 ml  $\text{H}_2\text{O}_2$  was added into the flask, the colour of the solution turned to brilliant yellow, obtaining the S-PGO solution. The S-PGO solution was centrifuged by 10 wt% HCl to remove the impurities and then washed by deionized water until to neutral, and dried at 80  $^{\circ}\text{C}$  for 12 h.



**Scheme 1** Schematic representation of the synthesis of SN-PRGO

Sulfur and nitrogen co-doped porous graphene (SN-PRGO) was obtained by reducing S-PGO with hydrazine hydrate. In brief, 0.5 g S-PGO was added into 100 ml deionized water and dispersed by ultrasonication for 1 h. Thereafter, 5 ml hydrazine hydrate was added and magnetically stirred at room temperature over night, then heated at 80 °C for 6 h, and, finally, washed by deionized water until neutral and dried at 80 °C for 12 h, eventually acquiring SN-PRGO. For comparison, S-GO and SN-RGO were also prepared by using the same technical route from the natural graphite without KOH-etching treatment.

## 2.2 Characterization

The microstructure of the samples was observed using a JEM-2010 transmission electron microscopy (TEM) at 200 kV. X-ray diffraction (XRD) patterns between 5 (2 $\theta$ ) and 60 (2 $\theta$ ) degrees were collected by Rigaku D/MAX-2500 powder diffractometer with Cu-K $\alpha$  radiation ( $\lambda=0.154$  nm) operated at 40 kV and 200 mA. Gas adsorption/desorption analysis was done in an ASPA 2020 system with N<sub>2</sub> as adsorbent at 77 K. Prior to analysis, samples were degassed in vacuum at 200 °C for 8 h. The SSA and micropore volume were calculated by the Brunauer–Emmett–Teller (BET) method and t-plot method, respectively. The pore size distribution was determined from the adsorption branch of the isotherm based on the Density Functional (DFT) method. X-ray photoelectron spectroscopic (XPS) measurements were conducted on a K-Alpha (Thermo VG Corporation, USA) using Al-K $\alpha$  radiation (1486.6 eV, 15 kV, 10 mA, 150 W). Prior to fitting, the Shirley background was subtracted. All binding energies (BEs) were corrected by charging of the samples by calibration on the graphitic carbon C1s peak at BE of 284.6 eV as a reference.

## 2.3 Preparation of electrode and electrochemical measurement

Electrochemical investigations were carried out in a three electrode system using platinum and Hg/HgO as the counter and reference electrode, respectively. And 6 M KOH solution was used as electrolyte. The working electrodes were prepared as follows: briefly, 80 wt% of the electrochemical active material, 10 wt% of carbon black and 10 wt% of polytetrafluoroethylene (PTFE) was dispersed in ethanol. Then the slurry was smeared into nickel foam and dried in vacuum at 120 °C for 10 h. The loading mass of the electrode is around 3 mg with an area of 1  $\times$  1 cm<sup>2</sup>. Cyclic voltammograms (CVs) and electrochemical impedance spectroscopy (EIS) were collected on CHI650D electrochemical workstation in a potential range of –1 to 0 V. The scan speeds for all CV tests were in range of 5–500 mV s<sup>-1</sup>. The galvanostatic

charge/discharge tests were carried on potentiostat/galvanostat (CT2001A, Land, Wuhan, China).

## 3 Results and discussion

Figure 1 shows the XRD patterns of the S-GO, S-PGO, SN-RGO and SN-PRGO samples, respectively. It is clear that only one diffraction peak at  $\sim 10^\circ$  (2 $\theta$ ) is visible on the XRD patterns of S-GO and S-PGO, behaving a typical GO structural feature [17]. Compared with that of S-GO, however, this diffraction peak of S-PGO becomes dramatically weaker and broadened, indicating a poor ordering of the graphite sheets, which can be ascribed to the introduction of pores or defects on the graphite sheets by the KOH-etching [18]. Furthermore, the diffraction peak of S-PGO shifts from 2 $\theta=12.0^\circ$  (S-GO) to a smaller angle of 2 $\theta=10.4^\circ$ , suggesting an enlarged interlayer space. As for the XRD pattern of SN-RGO, there occurs a broad and weak (002) peak at around 2 $\theta=23^\circ$ . However, this (002) peak becomes almost invisible in the SN-PRGO pattern, implying the relatively weaker restacking of the graphene sheets, which will be beneficial to ion transport and storage for supercapacitor application.

Typical TEM images of the S-GO, S-PGO, SN-RGO and SN-PRGO samples are displayed in Fig. 2. It can be seen that both S-GO and S-PGO exhibit a transparent GO feature (Fig. 2a, b). Besides, there can be observed some nano-sized pores in the S-PGO sheets (Fig. 2c), which should be originated from the etching of KOH to the carbon structure in natural graphite. This porous structure of SN-PRGO will offer more channels for electrolyte ions transport in through-plane directions of graphene sheets, which will be beneficial to the improvement of the supercapacitive performance [15]. Additionally, in comparison to SN-RGO, more wrinkling and folding can be observed in SN-PRGO (Fig. 2d, e). The surface wrinkling and folding can not only generate lots of

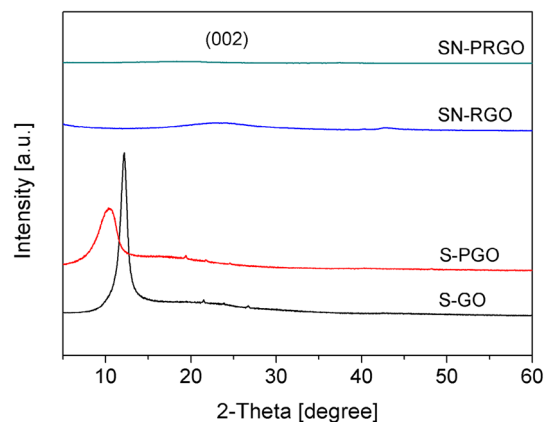
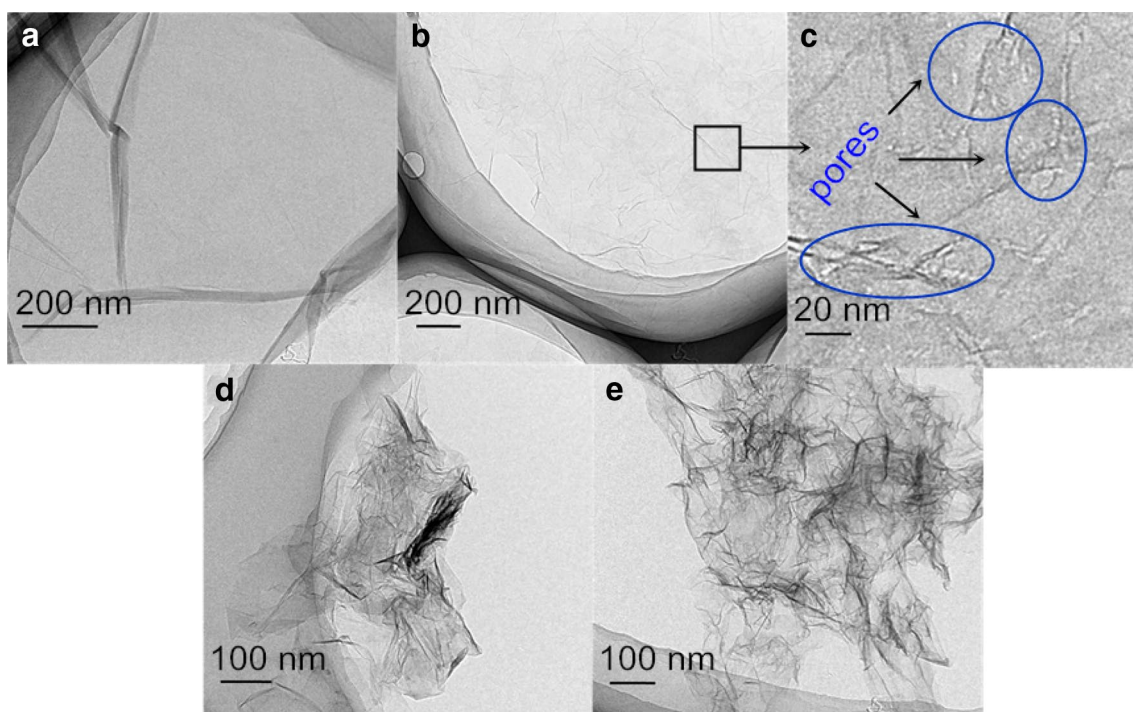


Fig. 1 XRD patterns of S-GO, S-PGO, SN-RGO and SN-PRGO



**Fig. 2** TEM images of **a** S-GO, **b**, **c** S-PGO, **d** SN-RGO, and **e** SN-PRGO, respectively

open edge sites [19], which is favorable for the ions transportation, but also prevent the aggregation of graphene sheets, which thus will facilitate the surface utilization of SN-PRGO.

The nitrogen adsorption/desorption isotherms and the corresponding pore size distributions of SN-RGO and SN-PRGO provide further evidences for the effect on the pore structure in the graphene brought by the KOH-etching

treatment to the parent graphite (Fig. 3). The initial straight part of the nitrogen adsorption/desorption isotherm at low relative pressure ( $P/P_0$ ) corresponds to the micropore filling. Therefore, the relatively longer straight part suggests the existence of more micropores in SN-PRGO, which is evidenced by the calculated micropore volumes ( $0.03$  and  $0.21$   $\text{cm}^3 \text{g}^{-1}$  for SN-RGO and SN-PRGO, respectively, Table 1). In addition, SN-RGO and SN-PRGO both begin to

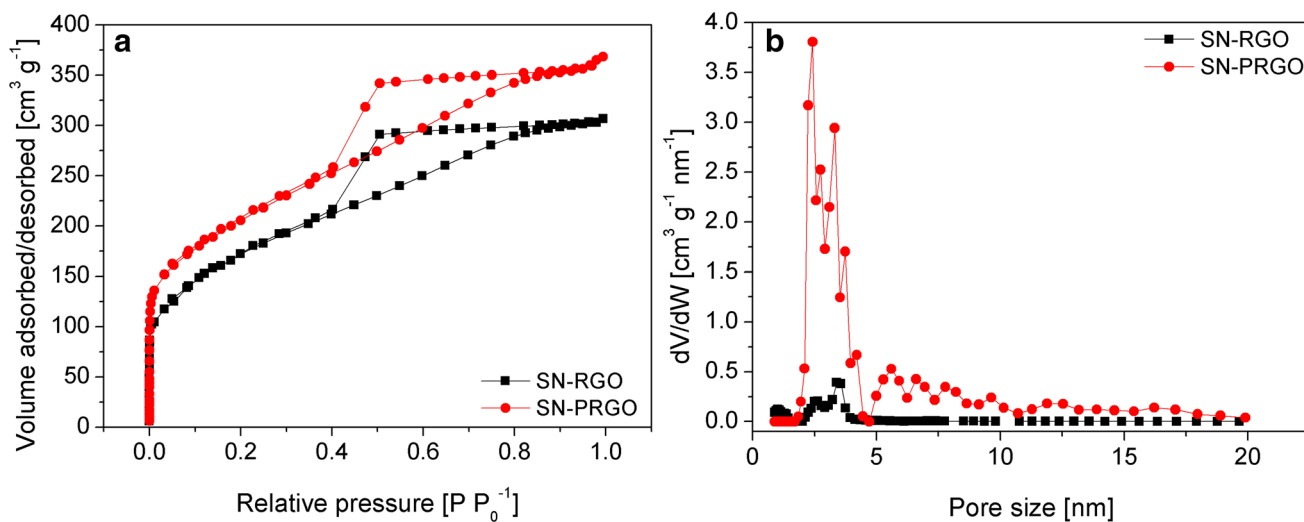


**Fig. 3** **a** Low-temperature nitrogen adsorption/desorption isotherms and **b** pore size distribution curves of SN-RGO and SN-PRGO, respectively

**Table 1** Porosity parameters of SN-RGO and SN-PRGO

Samples	$S_{\text{BET}}$ ( $\text{m}^2 \text{g}^{-1}$ )	$V_{\text{micro}}$ ( $\text{cm}^3 \text{g}^{-1}$ )	$V_{\text{meso}}$ ( $\text{cm}^3 \text{g}^{-1}$ )
SN-RGO	579.2	0.03	0.43
SN-PRGO	734.8	0.21	0.56

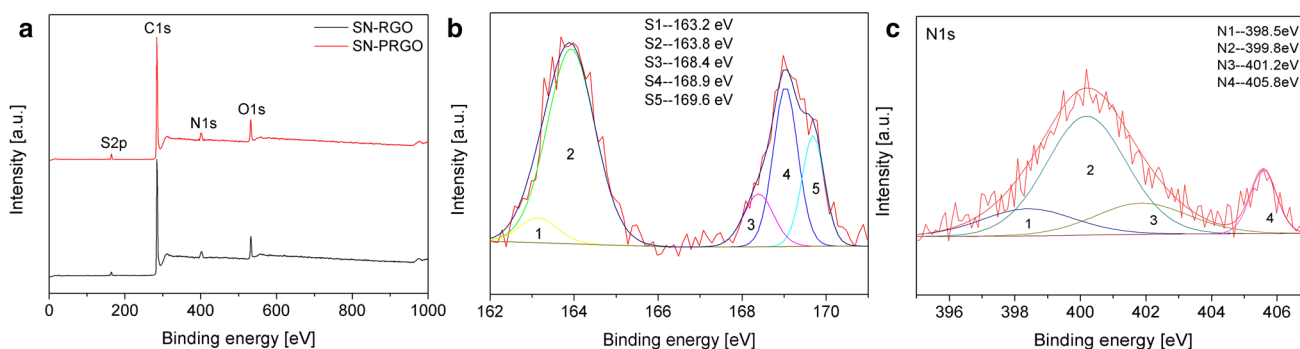
show a notable hysteresis loop at  $P/P_0 = 0.4$ , suggesting the existence of mesopores. Distinctly different from SN-RGO, however, SN-PRGO behaves a wider mesopore size distribution (Fig. 3b) and a larger mesopore volume (Table 1). SN-PRGO also exhibits a higher SSA value of  $734.8 \text{ m}^2 \text{g}^{-1}$ , significantly higher than that of SN-RGO ( $579.2 \text{ m}^2 \text{g}^{-1}$ ) (Table 1), which should be attributed to the increase in micropores and mesopores. Obviously, more developed pore structure and higher SSA value will be conducive to the superior supercapacitive performance of SN-PRGO.

X-ray photoelectron spectroscopy (XPS) was further used to characterize the surface chemistry of SN-RGO and SN-PRGO. A N1s (398.4 eV) peak and a S2p (168 eV) peak can be distinctly observed in the wide scan spectrum (Fig. 4a), confirming the existence of S and N in the SN-RGO and SN-PRGO samples. Obviously, the S-introduction should be ascribed to the sulfuric acid, which is used as the intercalant to prepare the graphite intercalation compound (GIC) from natural graphite. During the GIC preparation, the sulfuric acid will be intercalated into the graphite layers, and the sulfides will be grafted on the graphite surface [20, 21]. When the resultant GIC is thermally treated at  $1000^\circ\text{C}$ , these surface sulfides will be pyrolyzed, and the produced surface sulfur will be bound to the graphite layer [22]. As for the presence of N in both SN-RGO and SN-PRGO, it can be attributed to the hydrazine hydrate reduction. During the reduction process, nitrogen atoms in the hydrazine can be introduced into graphene lattice [23]. From the high resolution spectrum of S2p for SN-PRGO and SN-RGO (Fig. 4b and Figure S1a), it can be deduced that the S species are present as C–S–C species, which contain sulfur atoms that form thiophenic structures with neighboring carbon atoms

centered at 163.2 and 163.8 eV [10, 24], and oxidized sulfur species (–SO<sub>n</sub>–), which appear at higher binding energy of around 168.4–169.6 eV [25]. As for the N species in SN-PRGO and SN-RGO (Fig. 4c and Figure S1b), four types of N-containing groups can be fitted, including pyridine nitrogen, pyridine/pyrrolic nitrogen, graphitic/quaternary nitrogen and oxidized nitrogen, corresponding to the peaks located at 398.6, 400.4, 403.8, 407.4 eV, respectively [26–28].

The doped amounts of S and N in SN-RGO and SN-PRGO were also calculated according to the XPS analysis. Interestingly, more S (1.89 at%) and N (4.20 at%) are present in SN-PRGO, significantly higher than those of SN-RGO (1.36 at% S and 3.60 at% N) (Table S1). Obviously, the higher S and N contents in SN-PRGO should be related to the KOH-etching treatment on the natural graphite. The possible reason may be that the KOH-etching leads to the generation of abundant defects and activate sites in the graphite sheets, which will facilitate the bonding of heteroatoms to the graphite layer and thereby acquiring the loading of more heteroatoms in SN-PRGO.

The electrochemical performances of the samples are evaluated using a three-electrode system in 6 M KOH aqueous electrolyte. Figure 5a, b exhibits the representative cyclic voltammetry (CV) curves of SN-RGO and SN-PRGO at the scan rates ranging from 5 to  $500 \text{ mV s}^{-1}$ , respectively. It can be calculated from the integrated area of CV that the specific capacitance of SN-PRGO at the scan rate of  $5 \text{ mV s}^{-1}$  is up to  $438 \text{ F g}^{-1}$ , approximately 1.4 times higher than that ( $305 \text{ F g}^{-1}$ ) of SN-RGO. Compared with those of the heteroatoms doped carbon-based materials (Table 2), the specific capacitance of SN-PRGO is among the highest values, implying that the introduction of porosity in the parent graphite is beneficial to the electrochemical performance of the heteroatoms-doped graphene. The reason may be related to the following factors: (1) KOH etching to the parent graphite enables the as-prepared graphene to possess higher SSA and more developed pore structure (Fig. 3; Table 1), thereby facilitating the absorption of the

**Fig. 4** a XPS survey spectrum of SN-RGO and SN-PRGO, b, c high resolution spectrum of S2p and N1s of SN-PRGO, respectively

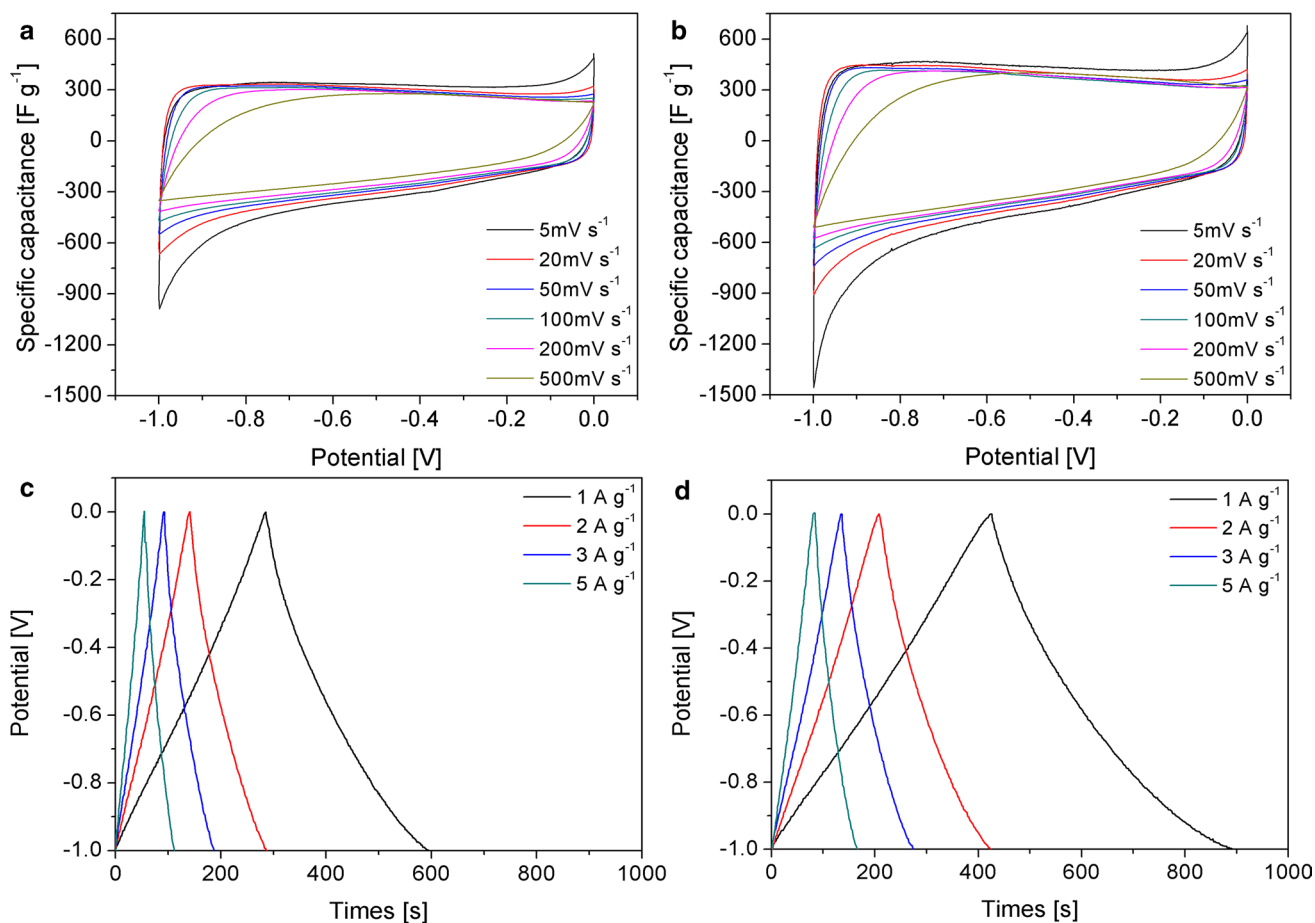


**Fig. 5** The CV curves of **a** SN-RGO and **b** SN-PRGO at versus scan rates ranging from 5 to 500  $\text{mV s}^{-1}$  with Hg/HgO as the reference electrode. The galvanostatic charging-discharging profiles of **c** SN-RGO and **d** SN-PRGO at different current densities, respectively

charge separated ions on the carbon surface and enhancing the EDLC capacitance; and (2) KOH etching to the parent graphite leads to the doping of more S and N in the as-prepared graphene, which can contribute both the pseudocapacitance through the redox reaction in the aqueous electrolyte and the EDLC capacitance by the improvement in wettability of electrolyte on the carbon surface [29]. Furthermore, SN-PRGO also exhibits better capacitance retention of 65% ( $289 \text{ F g}^{-1}$ ) at  $500 \text{ mV s}^{-1}$ , which is significantly higher than that 58% of SN-RGO ( $177 \text{ F g}^{-1}$ ). This result confirms that the pore structure of SN-PRGO facilitates the effective accessibility of electrolyte ions at high scan rates. This may be attributed to the existence of the more wrinkling and folding in SN-PRGO (Fig. 2e), which can effectively prevent the aggregation of graphene sheets and thus facilitate the fast ions transportation, and the pore-formation in the graphene sheets caused by KOH-etching to the parent graphite (Fig. 2c), which enables the as-prepared graphene to possess short diffusion channel for electrolyte ions in the through-plane direction, ensuring the fast ion diffusion in all directions.

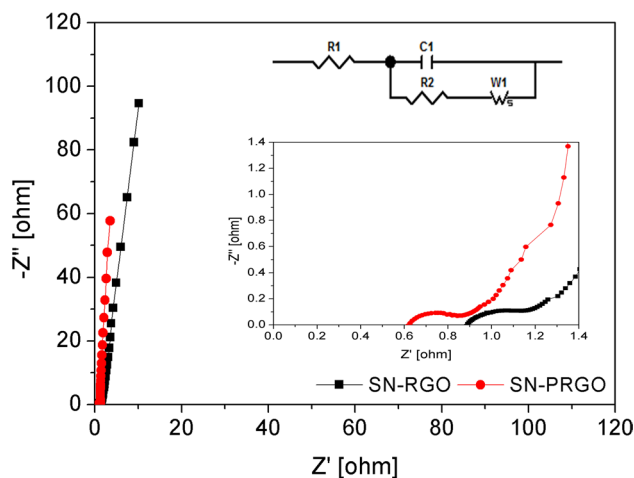
The galvanostatic charge/discharge curves of SN-RGO and SN-PRGO were tested at different current densities, as shown in Fig. 5c, d, respectively. The galvanostatic charge/discharge curves for the SN-RGO and SN-PRGO samples are not linear with time and give rise to some inflections, which further demonstrates that the doped heteroatoms could contribute additional pseudocapacitance to the total capacitive performance. However, the relatively longer charge/discharge time suggests that SN-PRGO can deliver higher specific capacitance than SN-RGO, which is in agreement well with the CV results. In addition, at the same current density, SN-PRGO can always behave a relatively smaller voltage drop (IR drop) at the initial portion of the discharge curve compared with SN-RGO (Figure S2), indicating a lower internal resistance [39]. This smaller IR drop of SN-PRGO in comparison to that of SN-RGO should be due to the more developed pore structures, especially the existence of the through-plane nanopores, which will lead to the decrease in these resistances with regard to the electrolyte diffusion and the ions migration.

**Table 2** Summary of capacitances of heteroatoms doped carbon-based materials in literatures

Carbon-based materials	C <sup>a</sup> (F g <sup>-1</sup> )	R <sup>b</sup>	EI <sup>c</sup>	References
S/N-graphene	402	5 mV s <sup>-1</sup>	6 M KOH	[12]
S/P-graphene aerogel	438	10 mV s <sup>-1</sup>	1 M H <sub>2</sub> SO <sub>4</sub>	[24]
N-graphene aerogel	290	1 A g <sup>-1</sup>	2 M KOH	[30]
N/P-activated graphene	204	0.2 A g <sup>-1</sup>	6 M KOH	[31]
N-mesoporous graphene	412	5 mV s <sup>-1</sup>	1 M H <sub>2</sub> SO <sub>4</sub>	[32]
N-mesoporous carbon	213	0.5 A g <sup>-1</sup>	6 M KOH	[33]
N/S-porous carbon	298	0.5 A g <sup>-1</sup>	6 M KOH	[34]
O/N-porous carbon	270	0.5 A g <sup>-1</sup>	1 M Na <sub>2</sub> SO <sub>4</sub>	[35]
N/O/P-porous carbon	206	0.1 A g <sup>-1</sup>	6 M KOH	[36]
B/N-porous carbon	304	0.1 A g <sup>-1</sup>	1 M H <sub>2</sub> SO <sub>4</sub>	[37]
B/O-carbon nanofiber	193	1 A g <sup>-1</sup>	1 M H <sub>2</sub> SO <sub>4</sub>	[38]
SN-PRGO	438	5 mV s <sup>-1</sup>	6 M KOH	This work

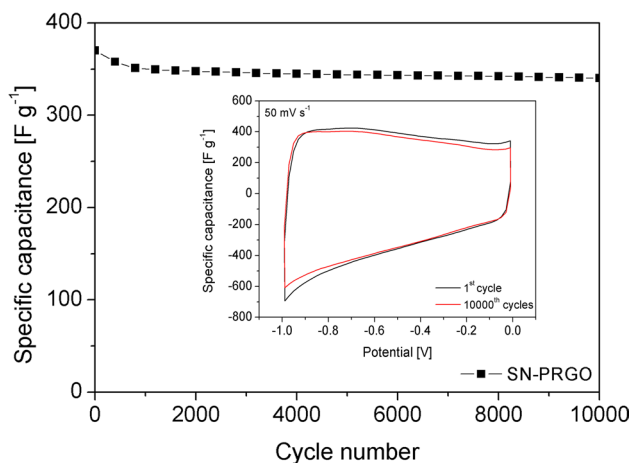
<sup>a</sup>Specific capacitance<sup>b</sup>Current density or scan rate<sup>c</sup>Electrolyte type

To get further insight into the different supercapacitive activity of SN-RGO and SN-PRGO, electrochemical impedance spectroscopy measurements are performed and shown in Fig. 6. The vertical line in the low frequency region is a result of the frequency dependence of ion diffusion at the electrode/electrolyte interface [22]. Compared to that of SN-RGO, the vertical line of SN-PRGO is more inclined to the imaginary axis in the low frequency region, indicating a superior capacitive behavior. Moreover, smaller semi-circle and shorter intercept with the real axis of SN-PRGO in comparison with those of SN-RGO (Fig. 6, inset) indicate the smaller interfacial charge transfer resistance and the ohmic resistance at the interface between electrode and electrolyte, respectively [40, 41]. The fitting equivalent circuit model is also shown in the inset of Fig. 6. The entire capacitor circuit consists of the equivalent series resistance (R1), the double layer capacitance (C), the interface resistance of ion adsorption/desorption on the electrode materials (R2), and the warburg resistance (W1), which is related to the electrolyte diffusion/transport in the electrode. According to the equivalent circuit, the decreasing charge transfer resistance (R2) and electrolyte diffusion impedance (W1) for SN-PRGO (Table S2) should be associated with rapid

**Fig. 6** The Nyquist plots of SN-RGO and SN-PRGO in 6 M KOH electrolyte (the inset are expanded high-frequency region of Nyquist plots and equivalent circuit, respectively)

ions transfer at the electrode/electrolyte interface due to the relatively more developed pore structure and the improved wettability with the KOH electrolyte.

The life cycle of the supercapacitor based on SN-PRGO electrode was tested at a constant scan rate of 50 mV s<sup>-1</sup>, as shown in Fig. 7. It can be found that SN-PRGO exhibits a slight decrement in the specific capacitance at the beginning, and then becomes stable with a small degradation over the entire cycle numbers. Besides, the CV curves of the electrode before and after 10,000 consecutive cycling test exhibit a similar shape without any obvious change (inset Fig. 7), with a capacitance retention of about 94%, reflecting a good electrochemical stability and a high degree of reversibility in the cycling test, which is significant for the practical application.

**Fig. 7** Cycling stability of SN-PRGO at 50 mV s<sup>-1</sup> in 6 M KOH electrolyte

## 4 Conclusion

Herein, we have successfully synthesized a sulfur and nitrogen co-doped porous graphene electrode, which is acquired through the pore-formation in the natural graphite, the preparation of sulfur doped porous graphite intercalation compounds (S-PGIC) and the construction of the sulfur/nitrogen co-doped porous reduced graphite oxide (SN-PRGO). In comparison to SN-RGO, SN-PRGO shows a significant increase in specific capacitance (from 305 to 438 F g<sup>-1</sup> in 6 M KOH electrolyte at the scan rate of 5 mV s<sup>-1</sup>) and a higher capacitance retention (~65% at the scan rate of 500 mV s<sup>-1</sup>, an approximately 7% improvement compared with SN-RGO). Moreover, SN-PRGO also exhibits a superior cycling stability (almost 94% specific capacitance can be retained even after 10,000 cycles). These outstanding electrochemical performances of SN-PRGO may be ascribed to its relatively higher SSA, more reasonable pore structure and more doped heteroatoms contributed by the pore-formation in the parent graphite.

**Acknowledgements** Financial supporting of this work by National Science Foundation of China (NSFC) (No. 50975247) and Hebei Natural Science Foundation (No. E2014203204) is acknowledged.

## References

- C. Xu, B. Xu, Y. Gu, Z. Xiong, J. Sun, X. Zhao, Graphene-based electrodes for electrochemical energy storage. *Energy Environ. Sci.* **6**, 1388–1414 (2013)
- C. Chen, Q. Zhang, M. Yang, C. Huang, Y. Yang, M. Wang, Structural evolution during annealing of thermally reduced grapheme nanosheets for application in supercapacitors. *Carbon* **50**, 3572–3584 (2012)
- L. Zhang, D. Huang, N. Hu, C. Yang, M. Li, H. Wei, Z. Yang, Y. Su, Y. Zhang, Three-dimensional structures of graphene/polyaniline hybrid films constructed by steamed water for high-performance supercapacitors. *J. Power Sources* **342**, 1–8 (2017)
- D. Liu, C. Fu, N. Zhang, H. Zhou, Y. Kuang, Three-dimensional porous nitrogen doped graphene hydrogel for high energy density supercapacitors. *Electrochim. Acta* **213**, 291–297 (2016)
- M. Lqbal, M. Hassan, M. Ashiq, S. Lqbal, N. Bibi, B. Parveen, High specific capacitance and energy density of synthesized graphene oxide based hierarchical AL2S3 nanorambutan for supercapacitor applications. *Electrochim. Acta* **246**, 1097–1103 (2017)
- P. Wang, H. He, X. Xu, Y. Jin, Significantly enhancing supercapacitive performance of nitrogen-doped graphene nanosheet electrodes by phosphoric acid activation. *ACS Appl. Mater. Interfaces* **6**, 1563–1568 (2014)
- Y. Wen, T. Rufford, D. Hulicova-Jurcakova, L. Wang, Nitrogen and phosphorous co-doped graphene monolith for supercapacitors. *Chem. Sus. Chem.* **9**, 513–520 (2016)
- J. Choi, M. Yang, S. Kim, Pseudocapacitive organic catechol derivative-functionalized three-dimensional graphene aerogel hybrid electrodes for high-performance supercapacitors. *Appl. Surf. Sci.* **422**, 316–320 (2017)
- X. Zhou, H. Li, J. Yang, Biomass-derived activated carbon materials with plentiful heteroatoms for high-performance electrochemical capacitor electrodes. *J. Energy Chem.* **25**, 35–40 (2016)
- X. Yu, H. Park, Sulfur-incorporated, porous graphene films for high performance flexible electrochemical capacitors. *Carbon* **77**, 59–65 (2014)
- M. Kota, X. Yu, S. Yeon, H. Cheong, H. Park, Ice-templated three dimensional nitrogen doped graphene for enhanced supercapacitor performance. *J. Power sources* **303**, 372–378 (2016)
- X. Zhang, P. Yan, R. Zhang, K. Liu, Y. Liu, T. Liu, X. Wang, A novel approach of binary doping sulfur and nitrogen into graphene layers for enhancing electrochemical performances of supercapacitors. *J. Mater. Chem. A* **4**, 19053–19059 (2016)
- C. Uthaisar, V. Barone, Edge effects on the characteristics of Li diffusion in graphene. *Nano Lett.* **10**, 2838–2842 (2010)
- L. Jiang, L. Sheng, C. Long, Z. Fan, Densely packed graphene nanomesh-carbon nanotube hybrid film for ultra-high volumetric performance supercapacitors. *Nano Energy* **11**, 471–480 (2015)
- Y. Gao, Y. Zhang, Y. Zhang, L. Xie, X. Li, F. Su, X. Wei, Z. Xu, C. Chen, R. Cai, Three-dimensional paper-like grapheme framework with highly orientated laminar structure as binder-free supercapacitor electrode. *J. Energy Chem.* **25**, 49–54 (2016)
- W. Hummers, R. Offeman, Preparation of graphitic oxide. *J. Am. Chem. Soc.* **80**, 1339–1339 (1958)
- C. Zheng, X. Zhou, H. Cao, G. Wang, Z. Liu, Synthesis of porous graphene/activated carbon composite with high packing density and large specific surface area for supercapacitor electrode material. *J. Power Sources* **258**, 290–296 (2014)
- J. Wang, S. Kaskel, KOH activation of carbon-based materials for energy storage. *J. Mater. Chem. A* **22**, 23710–23725 (2012)
- C. Zhang, N. Mahmood, H. Yin, F. Liu, Y. Hou, Synthesis of phosphorous-doped graphene and its multifunctional applications for oxygen reduction and lithium ion batteries. *Adv. Mater.* **25**, 4932–4937 (2013)
- M. Toda, A. Takagaki, M. Okamura, J. Knodo, S. Hayashi, K. Domen, S. Hayashi, M. Hara, Green chemistry: biodiesel made with sugar catalyst. *Nature* **438**, 178–178 (2005)
- M. Hara, Environmentally benign production of biodiesel using heterogeneous catalysts. *Chem. Sus. Chem.* **2**, 129–135 (2009)
- W. Kiciński, M. Szala, M. Bystrejewski, Sulfur-doped porous carbon: synthesis and applications. *Carbon* **68**, 1–32 (2014)
- B. Yuan, W. Xing, Y. Hu, X. Mu, J. Wang, Q. Tai, G. Li, L. Liu, K. Liew, Y. Hu, Boron/phosphorus doping for retarding the oxidation of reduced graphene oxide. *Carbon* **101**, 152–158 (2016)
- X. Yu, Y. Kang, H. Park, Sulfur and phosphorus co-doping of hierarchically porous graphene aerogels for enhancing supercapacitor performance. *Carbon* **101**, 49–56 (2016)
- Z. Yang, Z. Yao, G. Li, G. Fang, H. Nie, Z. Liu, X. Zhou, X. Chen, S. Huang, Sulfur-doped graphene as an efficient metal-free cathode catalyst for oxygen reduction. *ACS Nano* **6**, 205–211 (2012)
- W. Lu, M. Liu, L. Miao, D. Zhu, X. Wang, H. Duan, Z. Wang, L. Li, Z. Xu, L. Gao, L. Chen, Nitrogen-containing ultramicroporous carbon nanospheres for high performance supercapacitor electrodes. *Electrochim. Acta* **205**, 132–141 (2016)
- N. Gavrilov, I. Pašti, M. Vujković, J. Travas-Sejdic, G. Ćirić-Marjanović, S. Mentus, High-performance charge storage by N-containing nanostructured carbon derived from polyaniline. *Carbon* **50**, 3915–3927 (2012)
- N. Fechler, T. Fellingner, M. Antonietti, One-pot synthesis of nitrogen-sulfur-co-doped carbons with tunable composition using a simple isothiocyanate ionic liquid. *J. Mater. Chem. A* **1**, 14097–14102 (2013)
- W. Si, J. Zhou, S. Zhang, S. Li, W. Xing, S. Zhou, Tunable N-doped or dual N, S doped activated hydrothermal carbon



- derived from human hair and glucose for supercapacitor applications. *Electrochim. Acta* **107**, 397–405 (2013)
30. X. Su, L. Fu, M. Cheng, J. Yang, X. Guan, X. Zheng, 3D nitrogen-doped graphene aerogel nanomesh: Facile synthesis and electrochemical properties as the electrode materials for supercapacitors. *Appl. Surf. Sci.* **426**, 924–932 (2017)
  31. X. Sun, P. Cheng, H. Wang, H. Xu, L. Dang, Z. Liu, Z. Lei, Activation of graphene aerogel with phosphoric acid for enhanced electrocapacitive performance. *Carbon* **92**, 1–10 (2015)
  32. B. Wang, Y. Qin, W. Tan, Y. Tao, Y. Kong, Smartly designed 3D N-doped mesoporous graphene for high-performance supercapacitor electrodes. *Electrochim. Acta* **241**, 1–9 (2017)
  33. K. Wu, Q. Liu, Nitrogen-doped mesoporous carbons for high performance supercapacitors. *Appl. Surf. Sci.* **379**, 132–139 (2016)
  34. Y. Li, G. Wang, T. Wei, Z. Fan, P. Yan, Nitrogen and sulfur co-doped porous carbon nanosheets derived from willow catkin for supercapacitors. *Nano Energy* **19**, 165–175 (2016)
  35. B. Liu, Y. Liu, H. Chen, M. Yang, H. Li, Oxygen and nitrogen co-doped porous carbon nanosheets derived from perilla frutescens for high volumetric performance supercapacitors. *J. Power Sources* **341**, 309–317 (2017)
  36. J. Qu, C. Geng, S. Lv, G. Shao, S. Ma, M. Wu, Nitrogen, oxygen, and phosphorus decorated porous carbon derived from shrimp shell for supercapacitors. *Electrochim. Acta* **176**, 982–998 (2015)
  37. H. Chen, Y. Xiong, T. Yu, P. Zhu, X. Yan, Z. Wang, S. Guan, Boron and nitrogen co-doped porous carbon with a high concentration of boron and its superior capacitive behavior. *Carbon* **113**, 266–273 (2017)
  38. Z. Yu, L. Chen, L. Song, Y. Zhu, H. Ji, S. Yu, Free-standing boron an oxygen co-doped carbon nanofiber films for large volumetric capacitance and high rate capability supercapacitors. *Nano Energy* **15**, 235–243 (2015)
  39. M. Stoller, R. Ruoff, Best practice methods for determining an electrode material's performance for ultracapacitors. *Energy Environ. Sci.* **3**, 1294–1301 (2010)
  40. X. Zhang, X. Wang, L. Jiang, H. Wu, C. Wu, J. Su, Effect of aqueous electrolytes on the electrochemical behaviors of supercapacitors based on hierarchically porous carbons. *J. Power Sources* **216**, 290–296 (2012)
  41. B. Choi, J. Hong, W. Hong, P. Hammond, H. Park, Facilitated ion transport in all-solid-state flexible supercapacitors. *ACS Nano* **5**, 7205–7213 (2011)